Supporting Information

Mussel-Inspired Polydopamine-Coating for Enhanced Thermal Stability and Rate Performance of Graphite Anodes in Li-Ion Batteries

Seong-Hyo Park,[†] Hyeon Jin Kim,[†] Junmin Lee,[†] You Kyeong Jeong,[‡] Jang Wook Choi,[‡] and Hochun Lee*,[†]

[†] Department of Energy Systems Engineering, Daegu Gyeongbuk Institute of Science and Technology (DGIST), Daegu 42988 South Korea

[‡] Graduate School of Energy, Environment, Water, and Sustainability (EEWS) and KAIST Institute NanoCentury, Korea Advanced Institute of Science and Technology (KAIST), Daejeon 34141 South Korea

* Corresponding author

E-mail address: dukelee@dgist.ac.kr

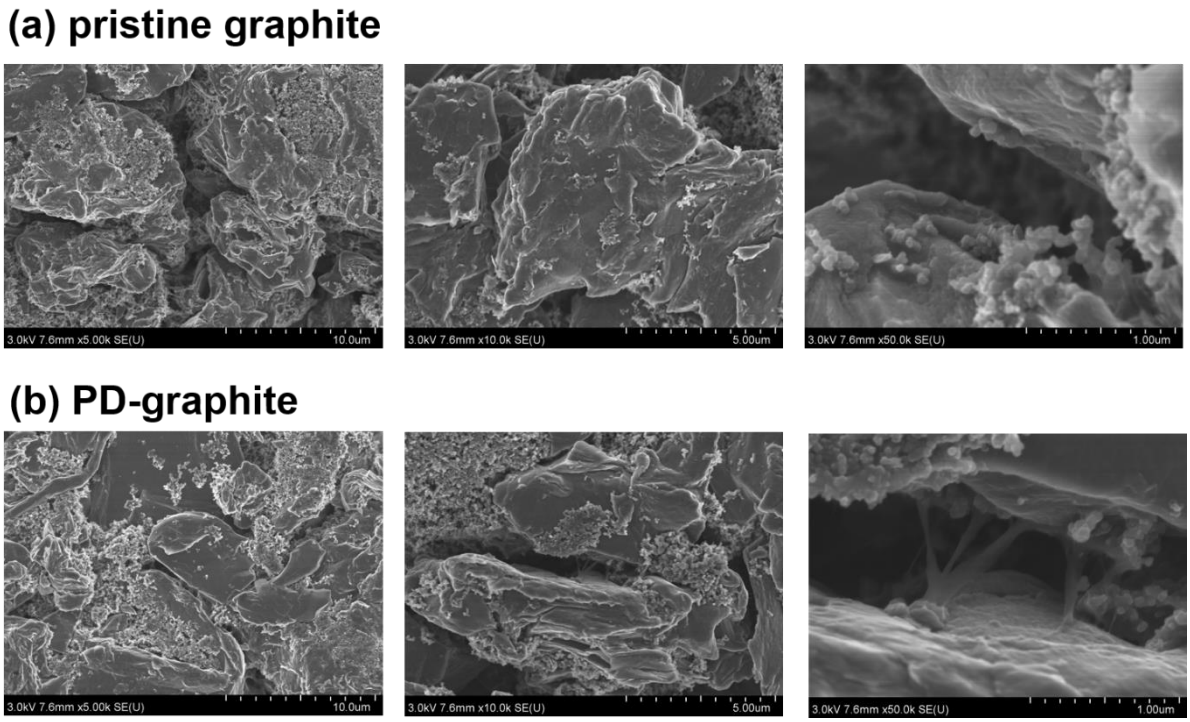

Figure S1. SEM images of the medium-loading (a) pristine and (b) PD-graphite electrodes. No discernable difference is notable between the two electrodes.

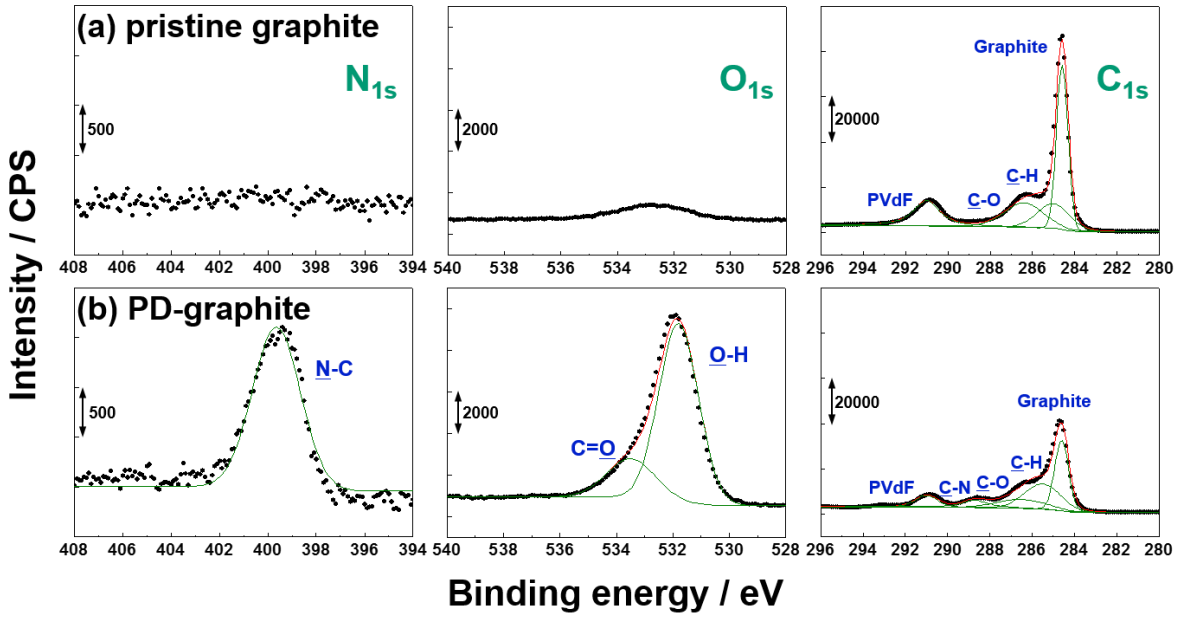

Figure S2. N1s, O1s and C1s XPS spectra of the uncycled medium-loading (a) pristine and (b) PD-graphite electrodes.

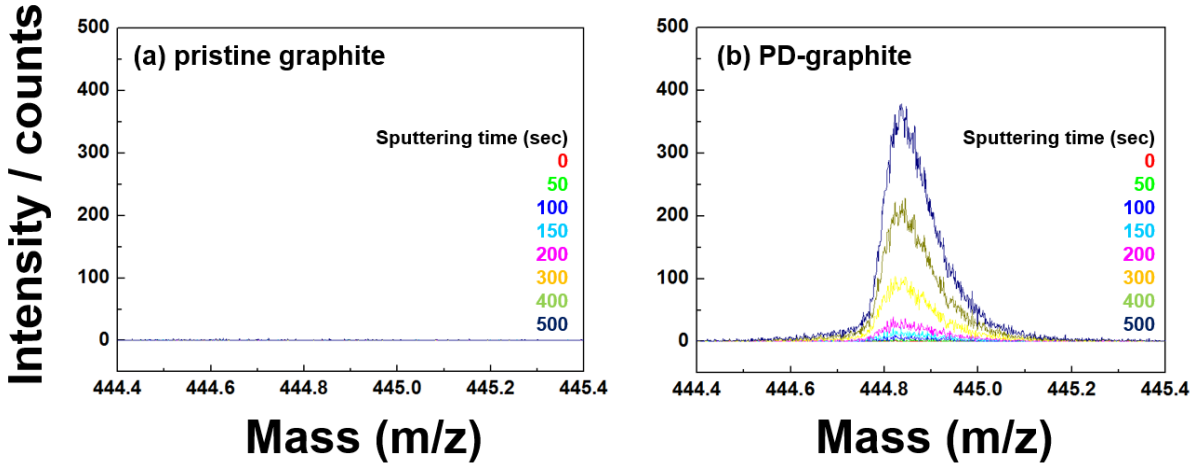

Figure S3. TOF-SIMS spectra of the cycled medium-loading (a) pristine and (b) PD-graphite electrodes.

TOF-SIMS measurement: Bi_3^{2+} (0.99 pA) accelerated at 30 keV was used as the analysis (primary) gun and Cs^+ (10.00 nA) accelerated at 0.25 keV, as the sputtering (secondary) gun. The depth profiling experiments were performed where the sputtering gun (Cs^+) was operated for 1.0 s over a 300 × 300 μm^2 area of the electrode surface followed by the analysis gun (Bi_3^{2+}) over a rastered 100 × 100 μm^2 area centered in the sputtering area. Fully delithiated pristine and PD-graphite anodes were collected from graphite/Li cells after being cycled three times in 1 M $LiPF_6$ EC/EMC (1/2, v/v) at 25 ^oC. The mass spectrum (b) clearly exhibits a peak at 445 (m/z) assigned to a trimer of 5,6-dihydroxyindole, possible fragment of PD.

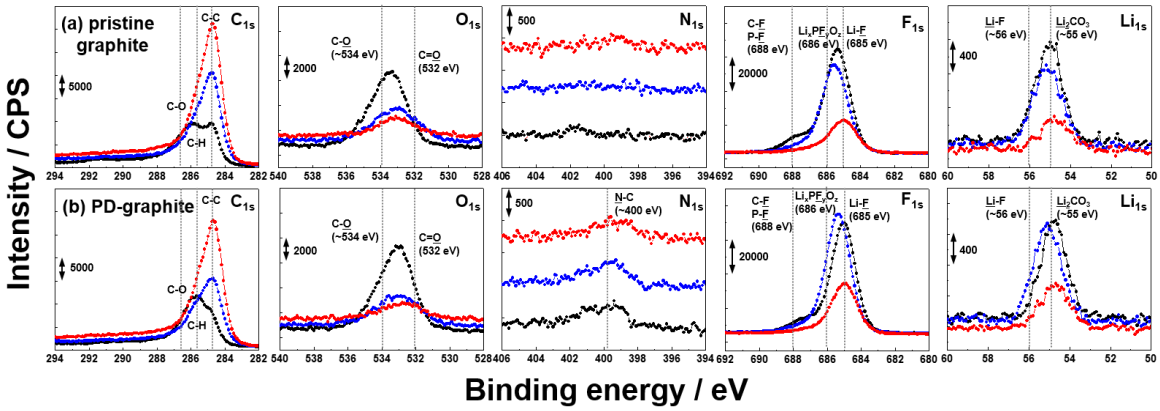

Figure S4. XPS spectra of the cycled medium-loading (a) pristine and (b) PD-graphite anodes. Fully delithiated pristine and PD-graphite anodes were collected from graphite/Li cells after being cycled three times in 1 M $LiPF_6$ EC/EMC (1/2, v/v). Sputtering time was 2 sec (black), 30 sec (blue), and 180 sec (red). The sputtering rate was 7 nm min^{-1} calibrated for SiO_2.

Peak assignment: The F1s peak at 685 eV is assigned to LiF and a peak at 686.3 eV to $LiPF_6$-derived products ($LiPF_6$/$LiP_xF_yO_z$). The Li1s spectrum displays a LiF peak at 55.5 eV and Li_2CO_3 peak at 54.5 eV. The C1s peaks at 284.5, 285, 286.5, 287.8, 288.5, and 290 eV are attributed to graphite, hydrocarbon, C-O, O-C-O, O-C=O, and Li_2CO_3, respectively. The O1s peaks at 532 and 533 eV are assigned to O-C=O/Li_2CO_3 and C-O/O-C-O, respectively. The PD-graphite shows a N_{1s} peak at around 399−401 eV, which is assigned to PD moiety.

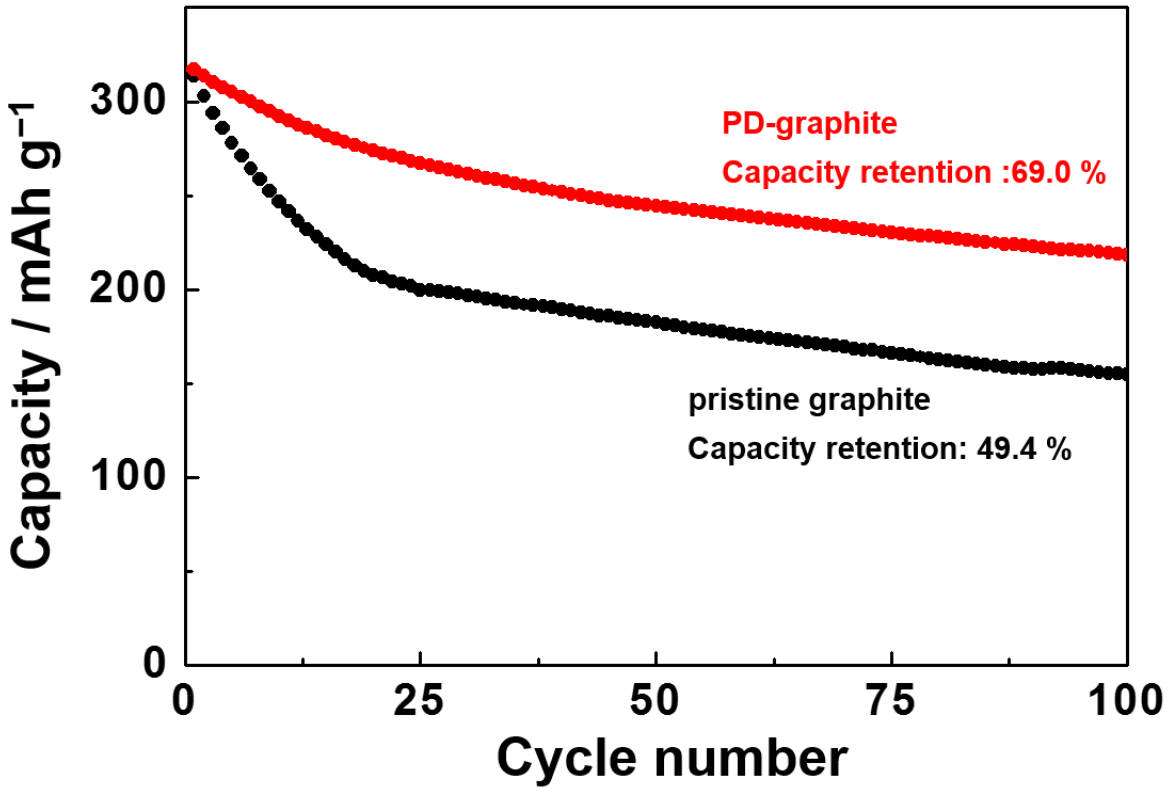

Figure S5. Cycle performances of the medium-loading pristine and PD-graphite symmetric cells at 60 ^{o}C. Charging and discharging with 0.5 C current followed by constant voltage between −0.5 V and +0.5 V.

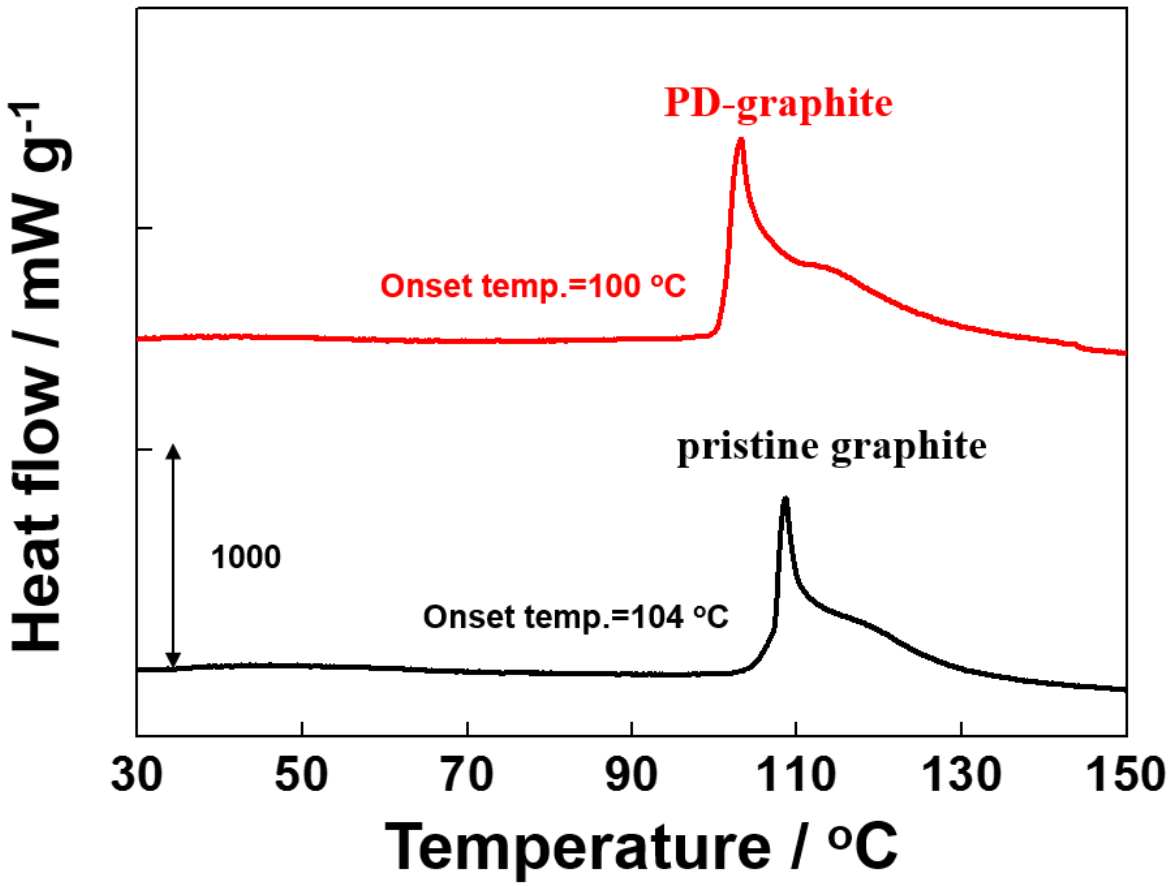

Figure S6. DSC curves of the fully delithiated graphite electrodes collected from the medium-loading pristine and PD-graphite/Li cells cycled in 1 M $LiPF_6$ EC/EMC (1/2, v/v).

Differential scanning calorimetry: The fully delithiated graphite samples were collected inside a glove box after 3 cycles over 1.5–0.005 V, and put into the Al pans without a washing process. There was no air-exposure during the sample preparation. The differential scanning calorimetry (DSC 131 EVO, SETARAM) measurements were performed with a heating rate of 5 $^{o}C\ min^{-1}$.

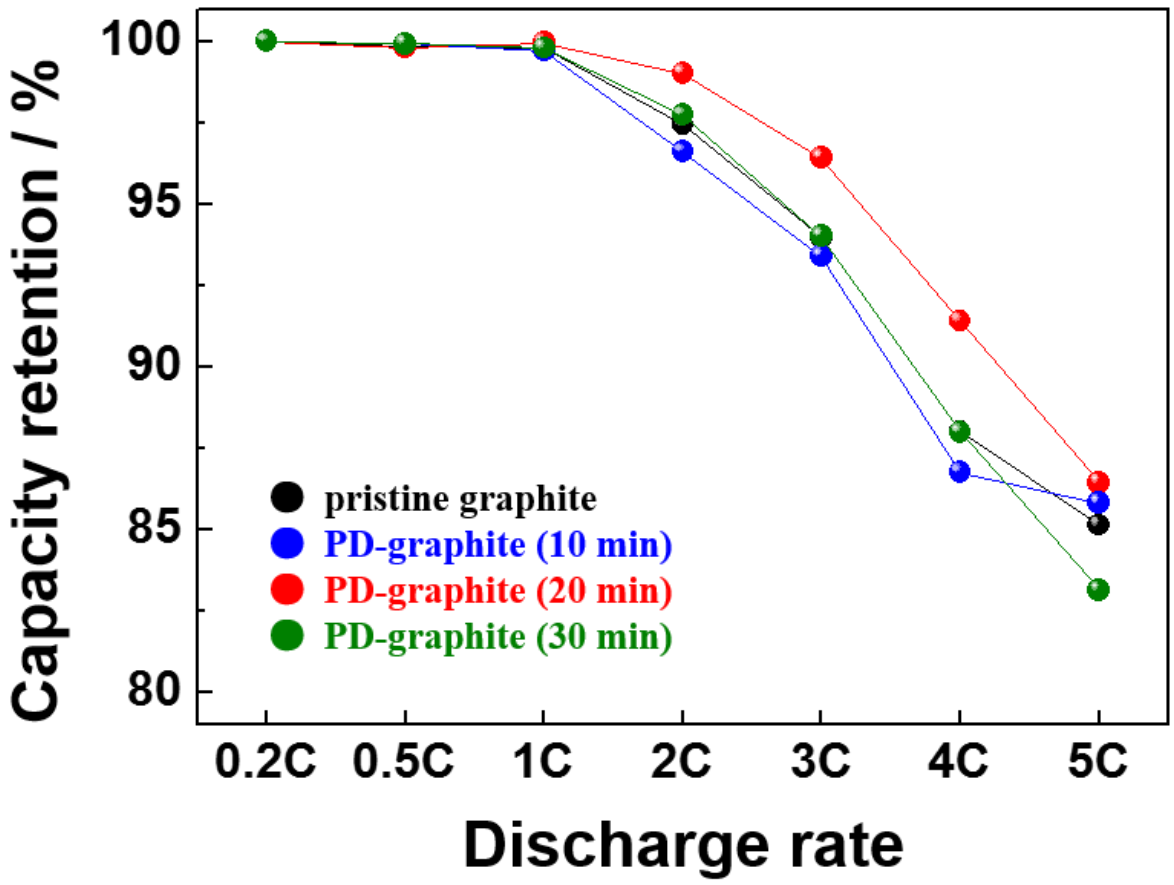

Figure S7. Discharge rate capability of the medium-loading pristine and PD-graphite/Li cells. The immersion times were 10 min (blue), 20 min (red), and 30 min (green).

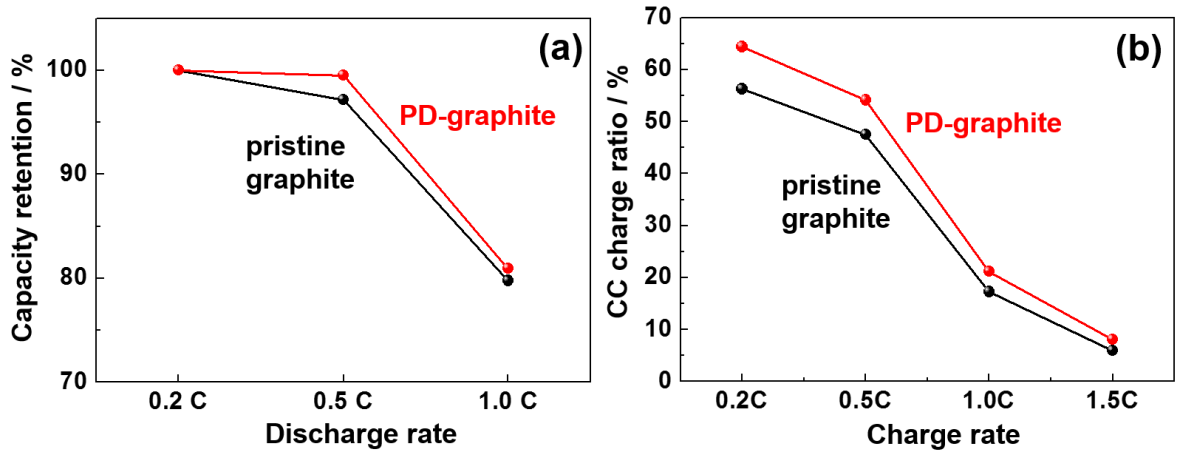

Figures S8. (a) Discharge rate capability of the high-loading pristine and PD-graphite/Li cells. (b) The CC charge ratio as a function of charge current rate. The discharge rate capability is shown only up to 1 C, because lithium dendrites growing at the counter electrode caused an internal short circuit at higher current rates.

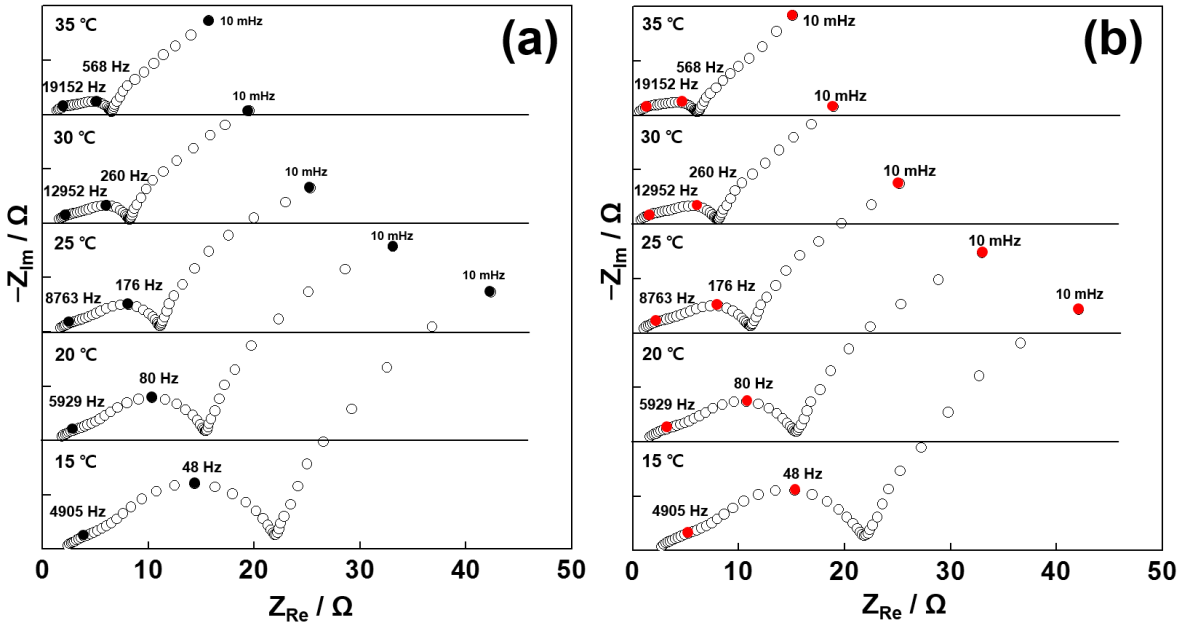

Figure S9. Nyquist plots of the medium-loading (a) pristine and (b) PD-graphite symmetric cells measured at 15–35 ^{o}C.

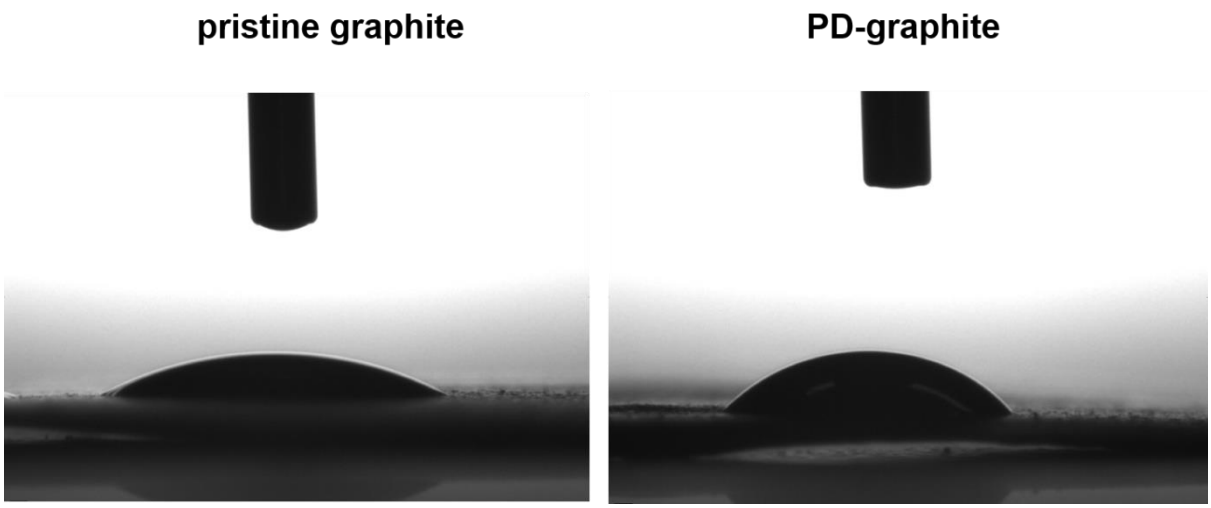

Figure S10. Contact angle images of diiodomethane on the high-loading (a) pristine and (b) PD-graphite electrodes.

SFE theory and measurement: The van-Oss-Chaudhury-Good (vOCG) theory allows us to retrieve the acid–base properties of solid surfaces, to account for the results of interfacial interactions.[1] Using the measured contact angle data (Table S3), three surface free energy (SFE) components were calculated. The vOCG model considers that solid SFE comprises the long-range interactions (London, Keesom, and Debye), called the Lifshitz-van der Waals component (γ^{AB}), and the short-range interactions, called the acid-base component (γ^{AB}). The latter component is further assumed to be $2(\gamma^{+}\ \gamma^{-})^{0.5}$, where γ^{+} and γ^{-} denote the Lewis acidic and basic constituents, respectively. As a result, the following relationship can be formulated:

$$\gamma^{Total} = \gamma^{LW} + \gamma^{AB} \quad (1)$$

$$\gamma^{AB} = 2(\gamma^{+}\ \gamma^{-})^{0.5} \quad (2)$$

As a consequence, a set of three probe liquids (i = 1, 2, 3) is required to obtain the three SFE components of a solid using the following equation:

$$0.5(1 + \cos\theta)\gamma_{L,i} = (\gamma_s^{LW}\gamma_{L,i}^{LW})^{0.5} + (\gamma_S^{+}\gamma_{L,i}^{-})^{0.5} + (\gamma_s^{-}\gamma_{L,i}^{+})^{0.5} \quad (3)$$

where θ denotes the contact angle, and the subscripts L and S refer to solid and liquid, respectively.

In this study, diiodomethane (D), formamide (F), and deionized water (W) were employed as the three probe liquids. For each liquid-electrode pair, the contact angle was measured more than ten times at different spots, and the lowest and the highest angle values were disregarded and the remaining values were used to calculate the arithmetic mean for the pair.

On the other hand, Owens-Wendt (OW) model considers only two SFE components: dispersive (γ^d) and polar (γ^p) SFE contributions, which corresponds to the γ^{LW} and γ^{AB} values of the vOCG model, respectively.[2]

$$\gamma^{Total} = \gamma^d + \gamma^p \quad (4)$$

In the OW model, a set of two probe liquids (one dispersive and one polar liquid) is employed, and the calculation of SFE is based on the following equation:

$$0.5(1 + \cos\theta)\gamma_{L,i} = (\gamma_s^{d}\gamma_{L,i}^{d})^{0.5} + (\gamma_S^{p}\gamma_{L,i}^{p})^{0.5} \quad (5)$$

REFERENCES

(1) Della Volpe, C.; Siboni, S. Acid-Base Surface Free Energies of Solids and The Definition of Scales in The Good-van Oss-Chaudhury Theory. *J. Adhes. Sci. Technol.* **2000,** 14, 235-272.

(2) Owens, D. K.; Wendt, R. C. Estimation of Surface Free Energy of Polymers. *J. Appl. Polym. Sci.* **1969,** 13, 1741-1747.

Table S1. Atomic ratios derived from XPS measurements for the uncycled pristine and PD-graphite electrodes.

	C [%]	O [%]	N [%]	F [%]
pristine graphite	77.9	1.4	0.0	20.7
PD-graphite	68.7	14.9	2.2	14.2

Table S2. Charge (Q_{ch}), discharge (Q_{dis}) capacities and the coulombic efficiencies (η_{1st}) at the first cycle of graphite/Li cells.

	Q_{ch} [mAh g^{-1}]	Q_{dis} [mAh g^{-1}]	η_{1st} [%]
pristine graphite	362.7	339.6	93.6
PD-graphite	363.3	341.5	94.0

Table S3. Contact angles measured on the high-loading pristine and PD-graphite electrodes using diiodomethane (D), formamide (F), and deionized water (W).

	D [^{o}]	F [^{o}]	W [^{o}]
pristine graphite	23.3	47.1	85.0
PD-graphite	34.9	67.9	105.7

Table S4. The fitted resistance values of the medium-loading pristine and PD-graphite symmetric cells measured at 15–35 ^{o}C.

	pristine graphite				PD-graphite			
Temperature [^{o}C]	R_S [Ω]	R_{SEI} [Ω]	R_{ct} [Ω]	$R_s+R_{SEI}+R_{ct}$ [Ω]	R_S [Ω]	R_{SEI} [Ω]	R_{ct} [Ω]	$R_s+R_{SEI}+R_{ct}$ [Ω]
15	2.39	4.43	14.90	21.72	2.73	4.43	14.39	21.55
20	1.82	4.28	8.84	14.94	1.65	3.64	9.55	14.84
25	1.73	3.94	5.30	10.97	1.15	3.14	6.72	11.01
30	1.57	3.01	3.51	8.09	0.79	1.96	4.95	7.70
35	1.35	2.09	2.53	5.97	0.68	1.61	3.55	5.84